ELSEVIER

Volume 184, Issue 1, January 2010

JOURNAL OF SOLID STATE CHEMISTRY

www.elsevier.com/locate/jssc

CONTENTS

Abstracted/indexed in BioEngineering Abstracts, Chemical Abstracts, Coal Abstracts, Current Contents/Physics, Chemical, & Earth Sciences, Engineering Index, Research Alert, SCISEARCH, Science Abstracts, and Science Citation Index. Also covered in the abstract and citation database SCOPUS®. Full text available on ScienceDirect®.

Regular Articles

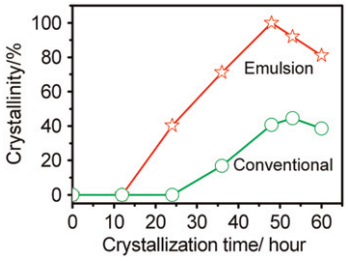

The nonionic emulsion synthesis allows rapid crystallization and morphological adjustment of zeolite ZSM-5 compared with the conventional hydrothermal synthesis.

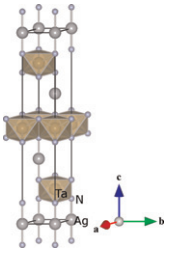

A delafossite silver nitride, $AgTaN_2$, was synthesized from $NaTaN_2$ by a cation-exchange reaction using a $AgNO_3$–NH_4NO_3 flux. It contains N–Ag–N linear bonding.

Regular Articles—Continued

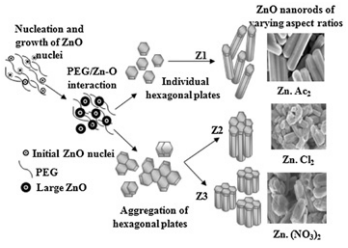

The study investigates the effect of Zn^{2+} ions derived from various zinc sources ($Zn \cdot Ac_2$, $Zn \cdot Cl_2$ and $Zn \cdot (NO_3)_2$) on the formation of one dimensional ZnO nanostructures with tunable aspect ratio.

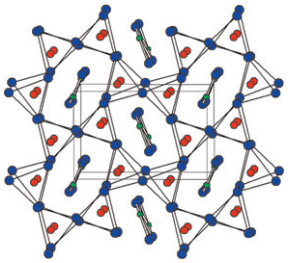

Tetrel (Si or Ge) and Bi atoms are arranged in an ordered manner in the β-Yb_5Sb_3-type structure adopted by RE_5TtBi_2.

Continued

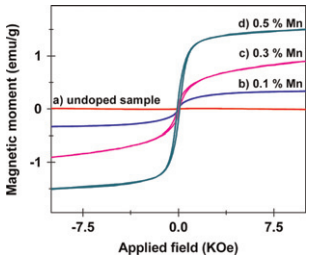

Room temperature ferromagnetic behavior was observed in the Cu_2O nanoflowers doped with Fe, Co, Ni and Mn ions. Cation deficiencies formed due to dopant ions were possibly responsible for ferromagnetism.

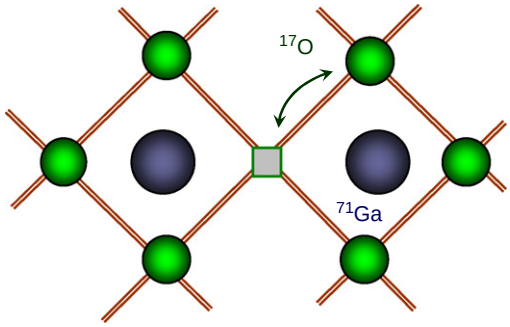

Up to 700 K the vacant oxygen sites are near Ga but not near Mg.

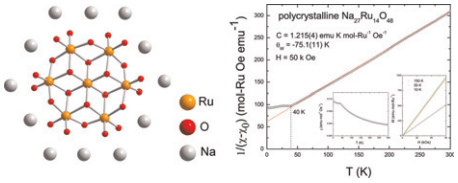

The basic building block in $Na_{27}Ru_{14}O_{48}$ is a heptameric plaquette. Magnetic susceptibility data indicate the presence of antiferromagnetic correlations.

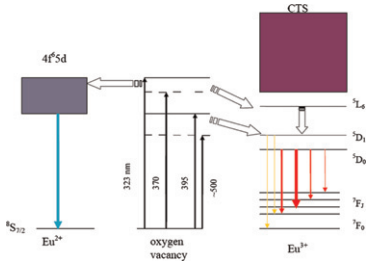

The scheme of nonradiative transfer over of energy of excitation from oxygen vacancies to ions Eu^{2+} and Eu^{3+} in $Sr_2Y_8(SiO_4)_6O_2$: Eu phosphors.

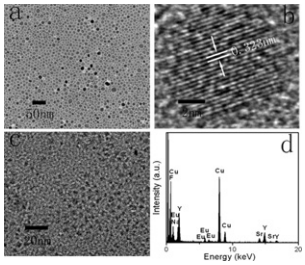

(a) TEM and (b) HRTEM images of $NaYF_4$:Sr(30%)/Eu(10%) nanocrystals. (c) TEM image of $NaYF_4$:Sr(70%)/Eu(10%) nanocrystals. (d) EDXA pattern of $NaYF_4$:Sr(30%)/Eu(10%) nanocrystals.

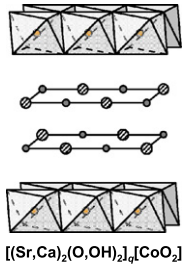

In the misfit-layered $[(Sr_{1-x}Ca_x)_2(O,OH)_2]_q[CoO_2]$ $(0.0 \le x \le 0.2)$ system the $x = 0$ phase has a commensurate match between the two layer blocks (i.e. $q = 0.5$), while isovalent Ca-for-Sr substitution induces lattice misfit (i.e. $q > 0.5$). At the same time Seebeck coefficient gets increased. Simultaneous increase in resistivity however outweighs this benefit, and accordingly the thermoelectric power factor is decreased.

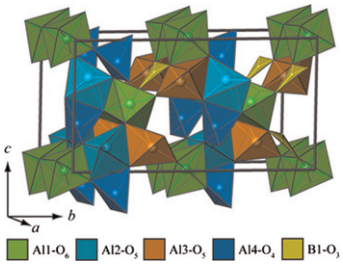

A chemical composition of $Al_{18}B_4O_{33} = Al_{4.91}B_{1.09}O_9 = 9Al_2O_3$: $2B_2O_3$ has been assumed for mullite-type aluminoborate with Al_5BO_9 structure. However, samples prepared by different routes showed compositions close to $5Al_2O_3$:B_2O_3.

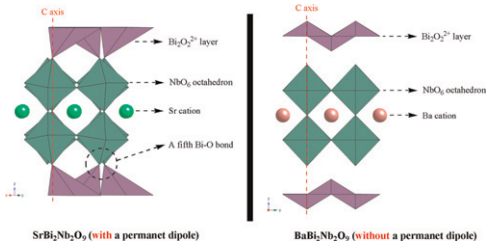

Aurivillius-type $ABi_2Nb_2O_9$ (A = Sr, Ba) photocatalysts were successfully synthesized by a citrate complex method. $SrBi_2Nb_2O_9$ and $BaBi_2Nb_2O_9$ showed different photocatalytic performances in the redox reaction of methyl orange (MO) under UV-light (λ = 254 nm), due to the different crystal structures of $ABi_2Nb_2O_9$ (A = Sr, Ba).

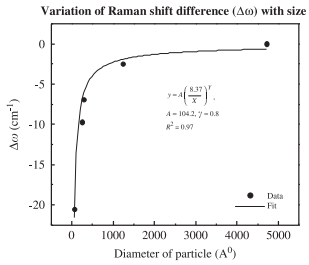

Variation of Raman shift difference ($\Delta\omega$) with size.

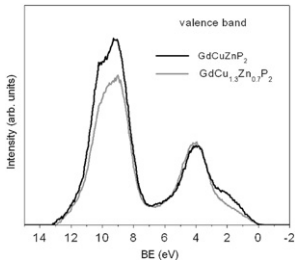

The absence of a band gap in the semimetallic quaternary rare-earth phosphides $RECuZnP_2$ permits the formation of a solid solution such as $GdCu_xZn_{2-x}P_2$ through hole-doping of the valence band.

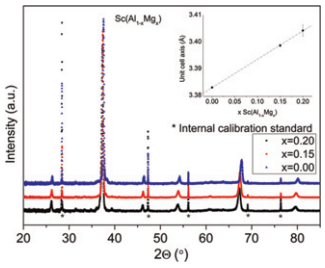

XRD pattern of $Sc(Al_{1-x}Mg_x)$. From the top: x = 0, 0.15, 0.20. The hydrogen absorption properties were studied by thermal desorption spectroscopy, pressure-composition-isotherms and scanning electron microscopy techniques.

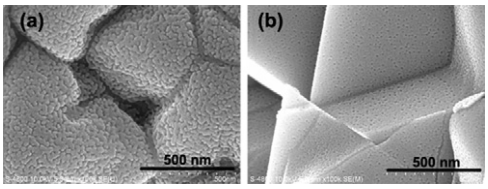

Representative nanostructure of $AgSbTe_2$ sample (a) ribbons obtained after melt spinning (b) bulk $AgSbTe_2$ material obtained after spark plasma sintering.

Continued

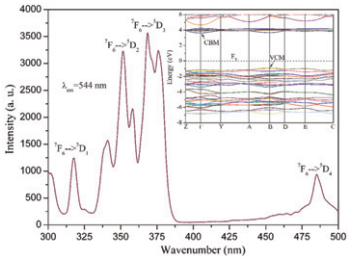

The metal–orthoborate framework of an $Li_3Sc(BO_3)_2$ is build up from ScO_6 octahedra connected to each other by sharing common edges, corners and faces of BO_3 units and LiO_4 groups. Large band gap of about 4.4 eV made Tb^{3+}-doped $Li_3Sc(BO_3)_2$ exhibits excellent photoluminescence property, given potential applications in phosphor-converted white light-emitting diodes.

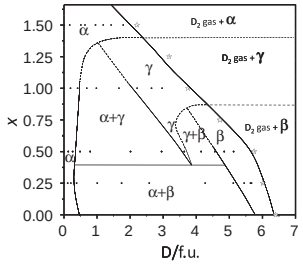

Phase diagram of the system $LaNi_{5-x}Pd_x$-D_2 (absorption) at 25 °C and 25 bar.

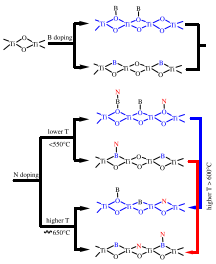

The changes of photocatalytic activity of B,N-TiO_2 with variable nitrogen doping temperatures are attributed to the transformation of surface structure and oxygen vacancies, and the Ti–O–B–N structure plays a vital role in photocatalytic activity under visible light irradiation.

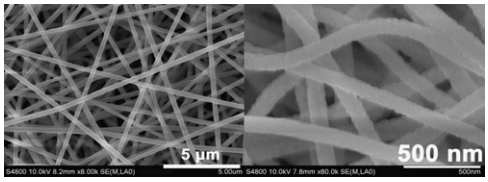

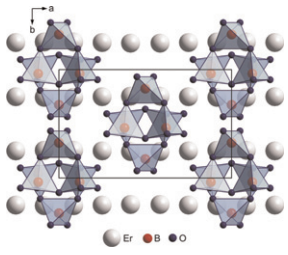

The first satisfying single-crystal structure determination of π-$ErBO_3$ sheds light on the extensively discussed structure of π-orthoborates. The application of light pressure during the solid state synthesis yielded in high-quality crystals, due to pressure-induced crystallization.

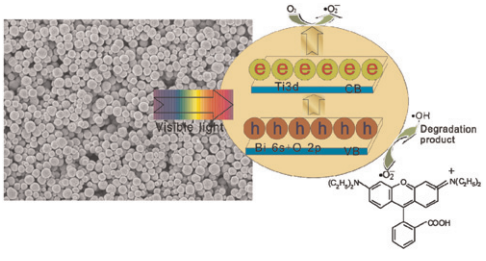

Bismuth titanate pyrochlore microspheres were synthesized by a facile hydrothermal process without the use of any surfactant or template, and the effects of concentration of OH^- on the diameter of microspheres, growth mechanism and photocatalytic properties were investigated.

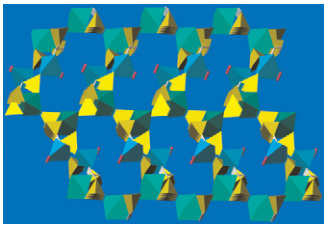

Two new zinc phosphonates with 3D open-framework consisting of 1D channels and blue or purple emission behave thermally stable up to 300 and 350 °C under air atmosphere, respectively.

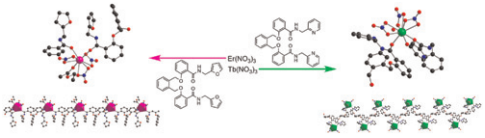

Two one-dimensional lanthanide coordination polymers were assembled by two structurally related bridging podands, and the effects of the structures on luminescent properties of the solid Tb(III) nitrate complexes were investigated.

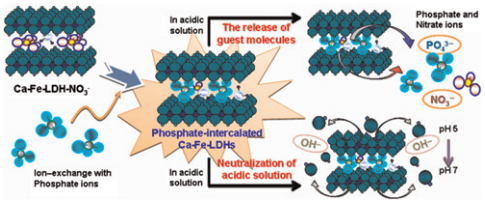

We synthesized phosphate-intercalated Ca–Fe-LDH materials that can act as bifunctional inorganic vectors for the slow release of phosphate fertilizer and also the neutralization of acid soil. Fitting analysis based on kinetic models indicated a heterogeneous diffusion process of phosphates and a distinct dependence of release rate on the charge of phosphates.

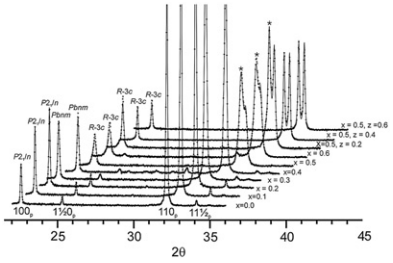

XRPD patterns for perovskite compounds along the lines $La_2Co(Mg_xTi_{1-x})O_6$ and $La_2Co_{1+z}(Mg_{0.5}Ti_{0.5})_{1-z}O_6$.

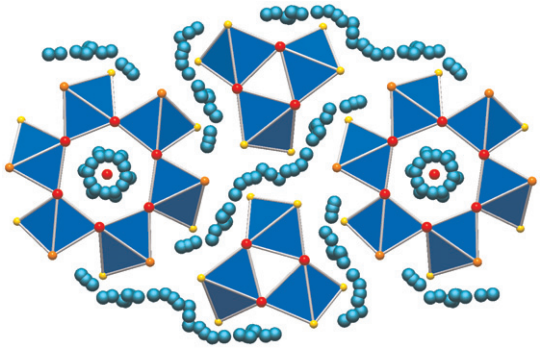

Copper cations easily move through the rigid tubular crystal structure of $Cu_{22}Bi_{12}S_{21}Cl_{16}$.

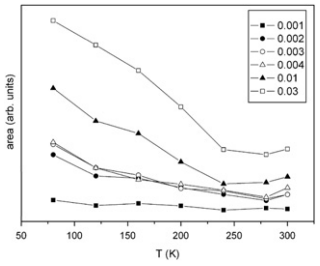

The ESR spectra reveal that the nature of Fe in $Sn_{1-x}Fe_xO_2$ samples is isolated rhombic Fe^{3+}-ion in rutile phase and the Fe content ($x = 0.01$ and 0.03), an extra spin-pumping is observed below 250 K.

Continued

Effects of calcination on microscopic and mesoscopic structures in Ca- and Sr-doped nano-crystalline lanthanum chromites

Himal Bhatt, J. Bahadur, M.N. Deo, S. Ramanathan, K.K. Pandey, D. Sen, S. Mazumder and Surinder M. Sharma

page 204

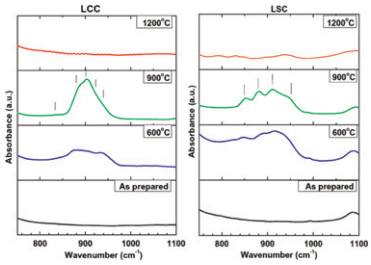

Dopant chromates evolve as intermediate phases during calcination of Ca- and Sr-doped nano-crystalline lanthanum chromites at intermediate temperatures, around 900 °C, evident from infrared spectroscopy. Such an event results in a modification of the microscopic and mesoscopic structures.

A new series of lanthanoid containing Keggin-type germanotungstates with acetate chelators: $[\{Ln(CH_3COO)GeW_{11}O_{39}(H_2O)\}_2]^{12-}$ {Ln = Eu^{III}, Gd^{III}, Tb^{III}, Dy^{III}, Ho^{III}, Er^{III}, Tm^{III}, and Yb^{III}}

Firasat Hussain, Stefan Sandriesser, Manfred Speldrich and Greta R. Patzke

page 214

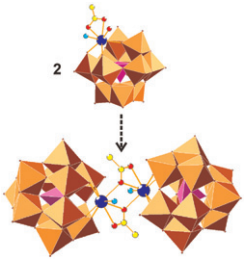

A new series of acetate-chelated lanthanoid containing germanotungstates $[\{Ln(CH_3COO)GeW_{11}O_{39}(H_2O)\}_2]^{12-}$ (Ln = Eu to Yb) is available from a convenient one-pot reaction. The influence of the lanthanide contraction on the structural properties is discussed and the magnetic properties of the Gd-representative are investigated in detail.

Stabilization of Th^{3+} ions into mixed-valence thorium fluoride

Marc Dubois, Belto Dieudonné, Adel Mesbah, Pierre Bonnet, Malika El-Ghozzi, Guillaume Renaudin and Daniel Avignant

page 220

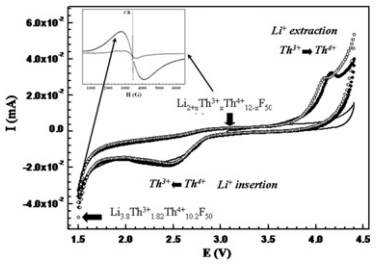

Electrochemical insertion of Li^+ ions into mixed-valence III/IV thorium fluoride and EPR spectra for the raw and inserted compounds.

Author inquiries

For inquiries relating to the submission of articles (including electronic submission where available) please visit this journal's homepage at http://www.elsevier.com/locate/jssc. You can track accepted articles at http://www.elsevier.com/trackarticle and set up e-mail alerts to inform you of when an article's status has changed. Also accessible from here is information on copyright, frequently asked questions and more.
Contact details for questions arising after acceptance of an article, especially those relating to proofs, will be provided by the publisher.

Language services. Authors who require information about language editing and copyediting services pre- and post-submission please visit http://webshop.elsevier.com/languageediting or our customer support site at http://support.elsevier.com. Please note Elsevier neither endorses nor takes responsibility for any products, goods or services offered by outside vendors through our services or in any advertising. For more information please refer to our Terms & Conditions http://www.elsevier.com/termsandconditions

For a full and complete Guide for Authors, please go to: http://www.elsevier.com/locate/jssc

Journal of Solid State Chemistry has no page charges.